

High-precision Penning trap mass measurements of neutron-rich chlorine isotopes at the $N = 28$ shell closure

H. Erington,^{1, 2, *} G. Bollen,^{1, 2} G. Dykstra,³ A. Hamaker,^{1, 2} C. M. Ireland,^{1, 2} C. R. Nicoloff,^{1, 2} D. Puentes,^{1, 2} R. Ringle,^{1, 2} S. Schwarz,¹ C. S. Sumithrarachchi,¹ A. A. Valverde,^{4, 5} and I. T. Yandow^{1, 2}

¹Facility for Rare Isotope Beams, East Lansing, Michigan, 48824, USA

²Department of Physics and Astronomy, Michigan State University, East Lansing, Michigan 48824, USA

³Department of Integrative Biology, Michigan State University, East Lansing, Michigan 48824, USA

⁴Physics Division, Argonne National Laboratory, Lemont, Illinois 60439, USA

⁵Department of Physics and Astronomy, University of Manitoba, Winnipeg, Manitoba MB R3T 2N2, Canada

(Dated: June 13, 2025)

Although it is known that the $N = 28$ spherical shell closure erodes, the strength of the closure with decreasing proton number $Z < 20$ is an open question in nuclear structure. In this region of interest, direct high-precision mass measurements of neutron-rich $^{43-45}\text{Cl}$ isotopes were performed at the Low Energy Beam and Ion Trap (LEBIT) when coupled to the National Superconducting Cyclotron Lab. The resulting mass excesses (MEs) are $\text{ME}^{(43)\text{Cl}} = -24114.4(1.7)$ keV, $\text{ME}^{(44)\text{Cl}} = -20450.8(10.6)$ keV, and $\text{ME}^{(45)\text{Cl}} = -18240.1(3.7)$ keV, and improve the uncertainty of these masses by up to a factor of ~ 40 compared to the previous values reported in the 2020 Atomic Mass Evaluation. Comparison to *ab initio* calculations using the Valence-Space In-Medium Similarity Renormalization Group (VS-IMSRG) shows good agreement up to and including the closure.

INTRODUCTION

The nuclear shell model, with “magic” numbers of increased stability, has been successful both theoretically and experimentally for decades. Originating from the addition of the Woods-Saxon potential and spin-orbit coupling term, the magic number shell closures appear at 2, 8, 20, 28, 50, 82, and 126 across the nuclear chart [1]. However, away from the valley of β -stability, we observe that magic numbers can shift or fade completely [2]. The experimental evidence for the erosion of the traditional magic numbers is key to our modern understanding of nuclear structure and the mechanisms that drive it [3].

A particular region of interest is near the doubly magic nucleus ^{48}Ca . One focus is understanding the strength of the neutron shell closure at $N = 28$ as the proton number, Z , decreases below 20, where there is the possibility for the erosion of the shell or the emergence of sub-shells. The magic number 28 is the first magic number produced from the spin-orbit interaction [1], allowing for insight into the contribution of this term. Furthermore, this region can be characterized in phenomenological shell-model calculations, offering quantifiable insight into the components of the nuclear interaction responsible for the structural evolution observed experimentally [4]. Specifically, recent valence-space formulation of the in-medium similarity renormalization group (VS-IMSRG) *ab initio* calculations [5] have shown agreement up to and at the drip line where experimental data are available. The VS-IMSRG and other models can be compared against new data in the $N = 28$ region as it is obtained [6-11].

From experimental studies of $\text{B}(E2; 2_1^+ \rightarrow 0_1^+)$ values in the silicon chain ($Z = 14$), it is known that the $N = 28$ spherical shell gap is eroded around ^{42}Si [12-15]. There is also evidence of both shape and configuration coexistence

in ^{44}S [16-22], which can indicate an “island of inversion” [23]. Despite the data available, this region is not fully described [24-26].

To fully characterize the erosion in the $N = 28$ region for $Z < 20$, chains of intermediate proton number must be studied and compared to theory. The isotopic chains of interest are argon ($Z = 18$), chlorine ($Z = 17$), sulfur ($Z = 16$), and phosphorus ($Z = 15$). These lie between the doubly magic ^{48}Ca and the spherical closure erosion occurring in ^{42}Si . In addition to $\text{B}(E2)$ values, the strength of a closure is also characterized by the trends of nuclear binding energies along isotopic chains. Improving our knowledge of binding energies requires precise mass measurements that reduce the uncertainty of present mass values and determine new masses far from β -stability.

Only two high-precision mass measurement results have been published in the $N = 28$ region along the isotopic chains of interest [11, 27]. In 2009, the Low Energy Beam and Ion Trap (LEBIT) [28], when coupled to the National Superconducting Cyclotron Lab (NSCL), measured the masses of neutron-rich $^{40-44}\text{S}$ isotopes [27]. These measurements improved the characterization of the sulfur chain up to $N = 28$ and are consistent with previous literature values; however, a large uncertainty remains for $N = 29$ and 30. In 2020, high-precision mass measurements of $^{46-48}\text{Ar}$ were performed with the ISOLTRAP mass spectrometer [29, 30] at ISOLDE/CERN [11]. The results find a persistent but slightly reduced shell closure compared to the calcium chain; however, the binding energy strength must also be considered alongside spectroscopic data and theoretical calculations [31, 32]. Importantly, these argon measurements cover $N = 28, 29, 30$, providing full characterization of the argon chain around $N = 28$ for mass

measurements. Other than these studies, only time-of-flight measurements have reached beyond $N = 28$ for all isotopic chains of interest, which have experimental uncertainties greater than 100 keV [33–35] that cannot reveal the closure’s strength. For this reason, precision mass measurements in this region of the nuclear chart are highly desirable to fully characterize the strength of the shell closure.

This work reports the first high-precision mass measurements of $^{43-45}\text{Cl}$ using the Time-of-Flight Ion Cyclotron Resonance (TOF-ICR) technique [36–38] at LEBIT. These measurements provide characterization up to $N = 28$, and the values are compared to previous measurements. Additionally, the new binding-energy trends are compared to the recent VS-IMSRG calculations to test agreement at $N = 28$.

EXPERIMENT

At the NSCL’s Coupled Cyclotron Facility, a ^{48}Ca primary beam was accelerated to 140 MeV/u and impinged on a ^9Be target of thickness 846 mg/cm². The produced fragments were sent through the A1900 fragment separator [39] to select the $^{43-45}\text{Cl}$ isotopes. After the separation, the beam proceeded via a momentum compression beamline to the gas stopping area. Before entering a gas cell, the beam was slowed with aluminum degraders and dispersion matched with an aluminum wedge. The effective thicknesses of the rotatable degraders were adjusted for each individual chlorine isotope to optimize stopping efficiency, allowing the beam to enter the gas cell at less than 1 MeV. The gas stopping area utilizes two gas cells, the Room Temperature Gas Cell (RTGC) [40] and the Advanced Cryogenic Gas Cell (ACGS) [41]. The gas cell used for each chlorine isotope was chosen based on the impurities and efficiency upon extraction.

In the RTGC or ACGS, the highly charged ions undergo collisions with the helium gas and the chlorine isotopes recombined down to a charge state of +1. In the RTGC the ions are transported by a combination of radiofrequency (RF) and direct current (DC) fields and gas flow. In the ACGS, the ions are transported via ion-carpet surfing [42] using an RF electric wave and a DC push field. In both gas cells, the ions are then extracted into an RF quadrupole (RFQ) ion guide. The gas stopping and LEBIT facilities are raised to 30 kV while the transport beam line between them is at ground potential. This configuration allows the ions to be accelerated to 30 keV during transport and then slowed before entering LEBIT. During transport, the ions are sent through a dipole magnet with a resolving power of approximately 1500, which selected all ion species based on the mass-to-charge ratio A/Q for the corresponding chlorine isotope, ensuring that bare $^{43}\text{Cl}^+$, $^{44}\text{Cl}^+$, and $^{45}\text{Cl}^+$ was delivered to LEBIT.

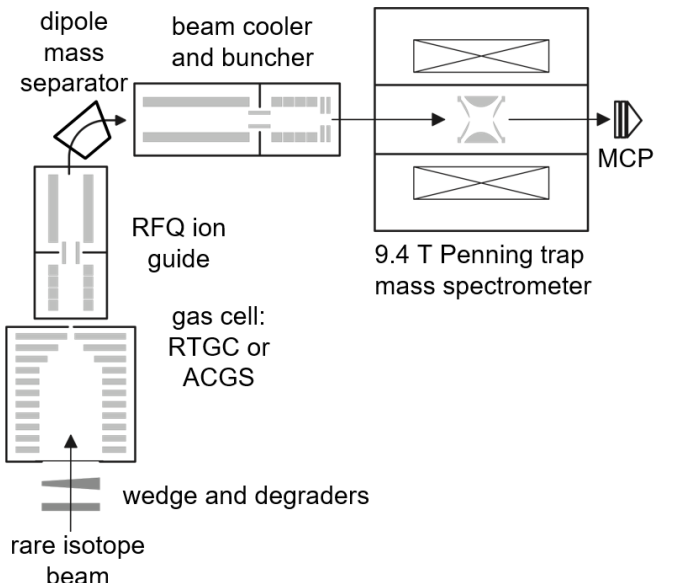


FIG. 1. Schematic of the NSCL gas cell and LEBIT facility.

After entering LEBIT, the selected continuous beam was injected into a linear buffer-gas-filled Paul trap cooler and buncher. Here, the beam is accumulated for a set duration, cooled with a He buffer gas, and then ejected in distinct ion bunches. Following extraction, the ion bunches are guided and injected into the 9.4 T Penning trap mass spectrometer [43]. Figure 1 shows a schematic of the gas cell and LEBIT facility.

Ions in the Penning trap are confined radially via a homogeneous magnetic field B and axially via a quadrupolar electrostatic field. While confined, the ions undergo three independent eigenmodes of motion resulting from the superposition of the two fields. Two of these occur in the radial plane of motion, ν_+ (reduced cyclotron frequency) and ν_- (magnetron frequency), and one in the axial plane, ν_z (axial frequency). Under typical operating conditions where the magnetic field is much stronger than the electrostatic field, $\nu_- \ll \nu_z < \nu_+$, and in an ideal trap, the approximation of the cyclotron frequency, ν_c , can be written as

$$\nu_c = \nu_- + \nu_+ = \frac{qB}{2\pi m} \quad (1)$$

where q is the charge of the ion, B is the strength of the magnetic field, and m is the mass of the ion. The error resulting from this approximation is negligible compared to the statistical errors [44] obtained in these measurements.

The masses of $^{43-45}\text{Cl}$ were determined by the Time-of-Flight Ion Cyclotron Resonance (ToF-ICR) technique. Ions extracted from the cooler-buncher were steered off-axis with Lorentz steerers [45], inducing initial magnetron motion upon capture in the trap. An azimuthal

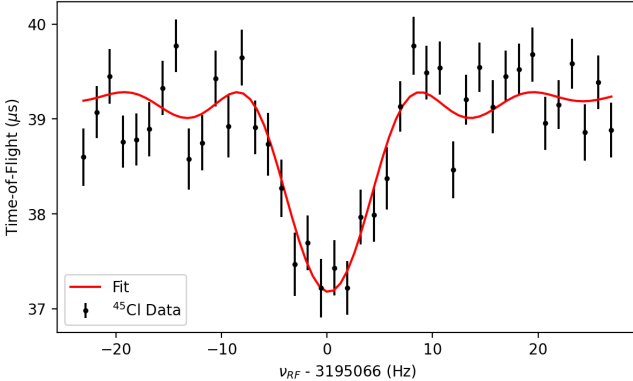


FIG. 2. A summed TOF spectrum for all of the ^{45}Cl measurements taken using the LEBIT 9.4 T Penning trap mass spectrometer. The spectrum is formed by 3789 ions. The width of the central dip corresponds to the inverse of the excitation time of $t_{RF} = 100$ ms. A χ^2 minimization fit to the analytical curve described in [38], depicted in red, was used to determine the frequency $\nu_{RF} = \nu_c$ occurring at the minimum time-of-flight.

quadrupolar RF field pulse ν_{RF} close to the expected cyclotron frequency is applied to the ions for a chosen excitation time, t_{RF} . In the case where $\nu_{RF} = \nu_c$, the slow magnetron motion is fully converted into the fast reduced cyclotron motion, increasing the radial kinetic energy of the ions. Upon ejection from the trap, ions move through the magnetic field gradient before striking the Multi-Channel Plate (MCP) detector. Ions with larger radial kinetic energy experience a greater force when moving through the magnetic field gradient due to their interaction with the magnetic moment, causing them to arrive at the MCP detector faster and, therefore, producing a shorter time of flight (TOF). Repeating the cycle of trapping, excitation, and measurement at different RF frequencies results in a resonance curve with a minimum at $\nu_{RF} = \nu_c$. An example of this resonance curve with the summed ^{45}Cl data is shown in Fig. 2.

A reference ion is needed to obtain the mass of the ion of interest. This reference enables the mass of the ion of interest to be determined relative to the reference mass via the cyclotron frequency ratio R ,

$$R = \frac{\nu_c}{\nu_{c,ref}} = \frac{q \cdot m_{ref}}{q_{ref} \cdot m} \quad (2)$$

where q and q_{ref} are the charges and m and m_{ref} are the masses of the ion of interest and the reference ion, respectively.

The final reported atomic mass M is found by taking the weighted average of all cyclotron frequency ratios, \bar{R} , and using

$$M = ([M_{ref} - m_e]/\bar{R}) + m_e \quad (3)$$

where M_{ref} is the atomic mass of the neutral reference atom/molecule and m_e is the electron mass. Electron binding energy is neglected as the statistical uncertainty of the measurement dominates.

For all measurements, reference ion measurements are interleaved with those of the ion of interest to obtain a linearly interpolated value of B at the time the ion of interest is measured. Seven independent measurements with $t_{RF} = 100$ ms were made of the $^{43}\text{Cl}^+$ ion using $^{39}\text{K}^+$ as the reference, of which the final three utilized the pulsed Ramsey resonance technique [46]. Seven independent measurements with $t_{RF} = 50$ ms were made of the $^{44}\text{Cl}^+$, using $^{12}\text{C}^{14}\text{N}^{16}\text{O}^{16}\text{O}^+$ ($A = 44$) and $^{39}\text{K}^+$ as references. Four independent measurements with $t_{RF} = 100$ ms of $^{45}\text{Cl}^+$ were made using $^{28}\text{Si}^{16}\text{O}^{16}\text{H}^+$ ($A = 45$) as the reference ion. Each measurement required between 20 min and 2 hr to produce a resonance curve, depending on the isotope.

RESULTS

The resulting difference of the frequency ratio for each individual measurement, R , from the mean frequency ratio, \bar{R} , for the series of measurements is shown in Fig. 3.

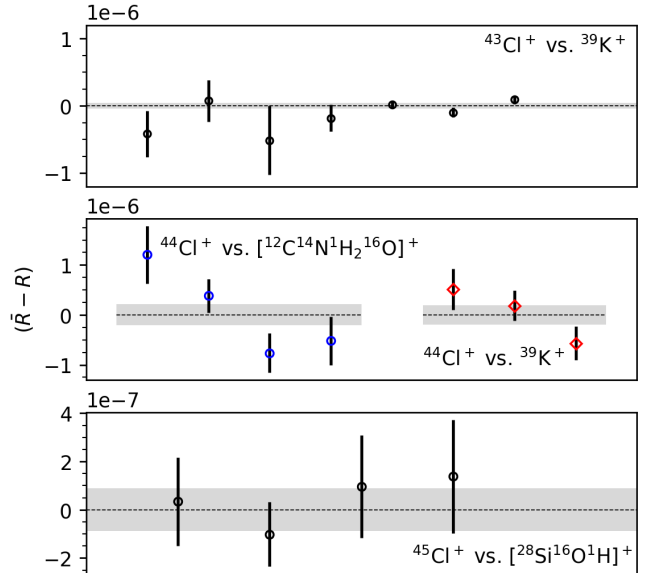


FIG. 3. Difference of the measured frequency ratio R from the mean ratio \bar{R} for each independent series of measurements. The data points are grouped by the reference ion, as indicated. Gray band shows the $\pm 1\sigma$ uncertainty in \bar{R} .

Several sources of systematic effects contribute to the uncertainty δ_R in \bar{R} . When $^{39}\text{K}^+$ is used as the reference ion, there is a mass difference of a few mass units between it and the ion of interest. It has been found that systematic shifts in \bar{R} (Eq. 3) scale linearly with

TABLE I. Mean ratios \bar{R} and the corresponding mass excesses calculated from the data shown in Fig. 3. Values from the AME2020 [47] are shown for comparison. Half-lives are taken from the NUBASE2020 evaluation [48].

Ion of Interest	Half-life	Reference	$\bar{R} = \nu_c / \nu_{c,ref}$	Mass Excess (keV)	
				This work	AME2020
$^{43}\text{Cl}^+$	3.13(9) s	$^{39}\text{K}^+$	0.906677379(40)	-24114.4(1.7)	-24159.5(61.8)
$^{44}\text{Cl}^+$	562(106) ms	$^{12}\text{C}^{14}\text{N}^{16}\text{O}^{16}\text{H}_2^+$	1.00080941(39)	-20453.0(16.1)	
		$^{39}\text{K}^+$	0.88597939(30)	-20448.6(14.0)	
		Average		-20450.8(10.6)	-20478.9(85.6)
$^{45}\text{Cl}^+$	413(25) ms	$^{28}\text{Si}^{16}\text{O}^1\text{H}^+$	0.999983276(89)	-18240.1(3.7)	-18262.5(136.1)

this mass difference, which is over an order of magnitude smaller than the statistical uncertainty. There are also mass-dependent shifts related to inhomogeneity in the magnetic field and trap imperfections, which have been studied at LEBIT in detail and are known to add $\delta_R \approx 2 \times 10^{-10} / u$ [49], as well as non-linear temporal shifts which contribute $\delta_R < 10^{-9}$ per hour [50]. To mitigate these, regular reference measurements were conducted. Isobaric contamination was mitigated using a dipolar RF excitation applied to the central ring electrode near their respective reduced cyclotron frequencies [51]. Finally, events with greater than six detected ions were discarded to avoid shifts from Coulomb interactions in the trap for all measurements.

The mean frequency ratios \bar{R} for each independent series of measurements are listed in Table I, along with their statistical uncertainties. Additionally, Fig. 4 shows the results compared to both the Atomic Mass Evaluation 2020 (AME2020) [47] and the previous measurements of these isotopes [33, 34]. Each measured isotope is less bound by 45.1(61.8) keV, 28.5(86.2) keV, and 22.4(136.2) keV than the AME2020 value, with an increased precision by a factor of 35, 8, and 36 for ^{43}Cl , ^{44}Cl , and ^{45}Cl respectively.

DISCUSSION

The mass values obtained in this work agree well with the AME2020 and are more precise, see Table I. Using these newly obtained masses, an evaluation of the neutron shell gap up to $N = 28$ can be performed. In this evaluation, quantities known as mass filters are of interest, determined via mass differences. One such quantity is the three-point estimator of the pairing gap, defined as

$$\Delta_{3n}(N, Z) = \frac{(-1)^N}{2} [\text{ME}(N+1, Z) - 2\text{ME}(N, Z) + \text{ME}(N-1, Z)] \quad (4)$$

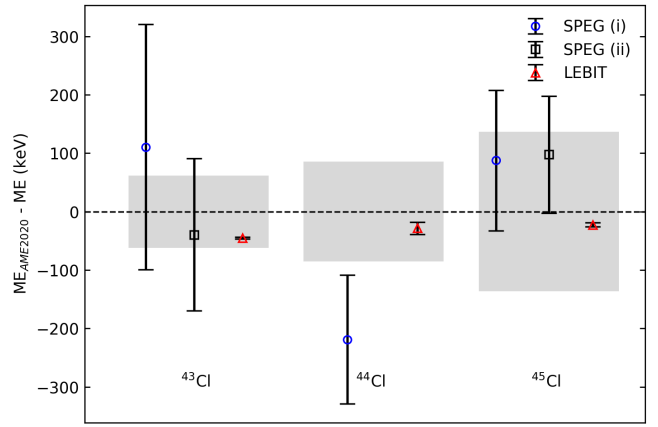


FIG. 4. Comparison between the values found for the $^{43-45}\text{Cl}$ mass excesses obtained in this work (red triangle) and previous works subtracting the experimental mass excess from the AME2020 mass excess. The gray band represents the AME2020 one standard deviation.

where ME denotes the mass excess of the respective isotope. This quantity is most commonly used to show the odd-even staggering effect. At the crossing of a shell closure, this staggering is enhanced and is related to the one-neutron shell gap via

$$\Delta_{1n}(N_{\text{closure}}, Z) = 2 \times \Delta_{3n}(N_{\text{closure}}, Z). \quad (5)$$

From this, one would expect a significant staggering enhancement at $N = 28$. Figure 5 shows the three-point estimator for the calcium, chlorine, and sulfur chains. The masses measured in this work contribute to the calculated values at $N = 25$ through $N = 29$ for the chlorine chain. The plot shows a decrease in the strength of the staggering for chlorine compared to calcium, while maintaining a greater strength compared to sulfur. This is what would be expected as the proton number decreases. However, it should be noted that the calculation for $N = 29$ still requires the use of two AME2020 values and due to the

larger uncertainty, the staggering may be more or less pronounced depending on the masses of ^{46}Cl and ^{47}Cl .

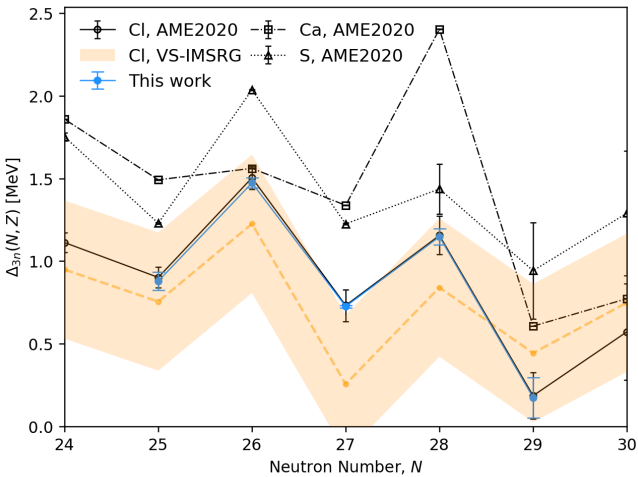


FIG. 5. The three-point estimator of the pairing gap ranging from $N = 24$ to $N = 30$ for different isotopes. Calcium ($Z = 20$) and sulfur ($Z = 16$) values are extracted from the AME2020 and are represented by open squares and triangles, respectively. Black circles represent chlorine ($Z = 17$) values from the AME2020, and the calculated values impacted by this work are shown as blue circles. VS-IMSRG calculation uncertainties are represented by the shaded orange region.

Additionally, comparing to theoretical models utilizing *ab initio* methods and modern theories of chiral effective field theory [52] in this region is critical considering that binding energy observables validate where these models are successful and where additional insight can be gained. Using the VS-IMSRG [53–56], agreement between theory and experiment was found for the argon chain in the $N = 28$ region [11, 56].

From updated VS-IMSRG calculations that use the 1.8/2.0(EM) NN+3N Hamiltonian and include a correction for systematic error through Bayesian analysis [5], the S_{1n} values and their errors were used to calculate the theoretical Δ_{3n} values for the chlorine chain based on Eq. 5, shown as the shaded region in Fig. 5. The plot shows that the trend in the calculation from the experimental data is consistent with the VS-IMSRG calculations, albeit with some offset within error, until the point at $N = 29$, where the error bar remains large due to the dominant contribution of the mass uncertainty for ^{46}Cl and ^{47}Cl . As such, precise mass measurements beyond $N = 28$ would be required to better characterize the shape of the three-point estimator of the pairing gap and the strength of the shell closure for the chlorine chain.

CONCLUSIONS

Penning trap mass measurements of $^{43–45}\text{Cl}$ were performed at LEBIT, improving the uncertainty of these iso-

topes by up to a factor of ~ 40 . The results are in agreement with previous values from the AME2020 and enable more precise determinations of nuclear structure effects using mass filters. Theoretical calculations and measurement calculations of the three-point estimator agree reasonably well. However, the large uncertainty from the less precise and unmeasured masses from AME2020 in the case of $N = 29$ does not yet allow the $N = 28$ shell closure strength to be determined with desirable accuracy. High-precision mass measurements of $^{46,47}\text{Cl}$, as well as measurements in the S and P isotope chains beyond $N = 28$, would bring clarity to this question. As of 2022, LEBIT is now coupled to the Facility for Rare Isotope Beams (FRIB), which can provide the necessary rates for high-precision measurements beyond $N = 28$ and down the isotopic chains of interest, making them within reach in the near future.

ACKNOWLEDGMENTS

This material is based upon work supported by the U.S. Department of Energy, Office of Science, Office of Nuclear Physics, and used resources of the Facility for Rare Isotope Beams (FRIB) Operations, which is a DOE Office of Science User Facility under Award Number DE-SC0023633. This work was conducted with the support of Michigan State University and the U.S. National Science Foundation under contracts nos. PHY-1565546 and PHY-2111185, the DOE, Office of Nuclear Physics under contract no. DE-AC02-06CH11357, DE-AC02-05CH11231, and DE-SC0022538. A.A.V acknowledges support from the DOE, Office of Nuclear Physics under contract no. DE-AC02-06CH11357 and NSERC (Canada), Application No. SAPPJ-2018-00028. C.M.I. acknowledges support from the ASET Traineeship under the DOE award no. DE-SC0018362.

* erington@frib.msu.edu

- [1] M. G. Mayer, On closed shells in nuclei. ii, *Phys. Rev.* **75**, 1969 (1949).
- [2] T. Otsuka, R. Fujimoto, Y. Utsuno, B. A. Brown, M. Honma, and T. Mizusaki, Magic numbers in exotic nuclei and spin-isospin properties of the NN interaction, *Phys. Rev. Lett.* **87**, 082502 (2001).
- [3] O. Sorlin and M.-G. Porquet, Nuclear magic numbers: New features far from stability, *Progress in Particle and Nuclear Physics* **61**, 602 (2008).
- [4] N. Smirnova, B. Bally, K. Heyde, F. Nowacki, and K. Sieja, Shell evolution and nuclear forces, *Physics Letters B* **686**, 109 (2010).
- [5] S. R. Stroberg, J. D. Holt, A. Schwenk, and J. Simonis, Ab initio limits of atomic nuclei, *Phys. Rev. Lett.* **126**, 022501 (2021).

[6] H. Scheit, T. Glasmacher, B. A. Brown, J. A. Brown, P. D. Cottle, P. G. Hansen, R. Harkewicz, M. Hellström, R. W. Ibbotson, J. K. Jewell, K. W. Kemper, D. J. Morrissey, M. Steiner, P. Thirolf, and M. Thoennessen, New region of deformation: The neutron-rich sulfur isotopes, *Phys. Rev. Lett.* **77**, 3967 (1996).

[7] S. Calinescu, L. Cáceres, S. Grévy, O. Sorlin, Z. Dombrádi, M. Stanoiu, R. Astabatyan, C. Borcea, R. Borcea, M. Bowry, W. Catford, E. Clément, S. Franchoo, R. Garcia, R. Gillibert, I. H. Guerin, I. Kuti, S. Lukyanov, A. Lepailleur, V. Maslov, P. Morfouace, J. Mrazek, F. Negoita, M. Niikura, L. Perrot, Z. Podolyák, C. Petrone, Y. Penionzhkevich, T. Roger, F. Rotaru, D. Sohler, I. Stefan, J. C. Thomas, Z. Vajta, and E. Wilson, Coulomb excitation of ^{44}Ca and ^{46}Ar , *Phys. Rev. C* **93**, 044333 (2016).

[8] R. Winkler, A. Gade, T. Baugher, D. Bazin, B. A. Brown, T. Glasmacher, G. F. Grinyer, R. Meharchand, S. McDaniel, A. Ratkiewicz, and D. Weisshaar, Quadrupole collectivity beyond $n = 28$: Intermediate-energy coulomb excitation of $^{47,48}\text{Ar}$, *Phys. Rev. Lett.* **108**, 182501 (2012).

[9] R. W. Ibbotson, T. Glasmacher, P. F. Mantica, and H. Scheit, Coulomb excitation of odd-a neutron-rich $\pi(s-d)$ and $\nu(f-p)$ shell nuclei, *Phys. Rev. C* **59**, 642 (1999).

[10] B. Longfellow, D. Weisshaar, A. Gade, B. A. Brown, D. Bazin, K. W. Brown, B. Elman, J. Pereira, D. Rhodes, and M. Spieker, Shape changes in the $n = 28$ island of inversion: Collective structures built on configuration-coexisting states in ^{43}S , *Phys. Rev. Lett.* **125**, 232501 (2020).

[11] M. Mousseot, D. Atanasov, C. Barbieri, K. Blaum, M. Breitenfeld, A. de Roubin, T. Duguet, S. George, F. Herfurth, A. Herlert, J. D. Holt, J. Karthein, D. Lunney, V. Manea, P. Navrátil, D. Neidherr, M. Rosenbusch, L. Schweikhard, A. Schwenk, V. Somà, A. Welker, F. Wienholtz, R. N. Wolf, and K. Zuber, Examining the $n = 28$ shell closure through high-precision mass measurements of $^{46-48}\text{Ar}$, *Phys. Rev. C* **102**, 014301 (2020).

[12] B. Bastin, S. Grévy, D. Sohler, O. Sorlin, Z. Dombrádi, N. L. Achouri, J. C. Angélique, F. Azaiez, D. Baborodin, R. Borcea, C. Bourgeois, A. Buta, A. Bürger, R. Chapman, J. C. Dalouzy, Z. Dlouhy, A. Drouard, Z. Elekes, S. Franchoo, S. Iacob, B. Laurent, M. Lazar, X. Liang, E. Liénard, J. Mrazek, L. Nalpas, F. Negoita, N. A. Orr, Y. Penionzhkevich, Z. Podolyák, F. Pougheon, P. Roussel-Chomaz, M. G. Saint-Laurent, M. Stanoiu, I. Stefan, F. Nowacki, and A. Poves, Collapse of the $n = 28$ shell closure in ^{42}Si , *Phys. Rev. Lett.* **99**, 022503 (2007).

[13] S. Takeuchi, M. Matsushita, N. Aoi, P. Doornenbal, K. Li, T. Motobayashi, H. Scheit, D. Steppenbeck, H. Wang, H. Baba, D. Bazin, L. Cáceres, H. Crawford, P. Fallon, R. Gernhäuser, J. Gibelin, S. Go, S. Grévy, C. Hinke, C. R. Hoffman, R. Hughes, E. Ideguchi, D. Jenkins, N. Kobayashi, Y. Kondo, R. Krücken, T. Le Bleis, J. Lee, G. Lee, A. Matta, S. Michimasa, T. Nakamura, S. Ota, M. Petri, T. Sako, H. Sakurai, S. Shimoura, K. Steiger, K. Takahashi, M. Takechi, Y. Togano, R. Winkler, and K. Yoneda, Well developed deformation in ^{42}Si , *Phys. Rev. Lett.* **109**, 182501 (2012).

[14] S. R. Stroberg, A. Gade, J. A. Tostevin, V. M. Bader, T. Baugher, D. Bazin, J. S. Berryman, B. A. Brown, C. M. Campbell, K. W. Kemper, C. Langer, E. Lunderberg, A. Lemasson, S. Noji, F. Recchia, C. Walz, D. Weisshaar, and S. J. Williams, Single-particle structure of silicon isotopes approaching ^{42}Si , *Phys. Rev. C* **90**, 034301 (2014).

[15] A. Gade, B. A. Brown, J. A. Tostevin, D. Bazin, P. C. Bender, C. M. Campbell, H. L. Crawford, B. Elman, K. W. Kemper, B. Longfellow, E. Lunderberg, D. Rhodes, and D. Weisshaar, Is the structure of ^{42}Si understood?, *Phys. Rev. Lett.* **122**, 222501 (2019).

[16] T. Glasmacher, B. Brown, M. Chromik, P. Cottle, M. Fauerbach, R. Ibbotson, K. Kemper, D. Morrissey, H. Scheit, D. Sklenicka, and M. Steiner, Collectivity in ^{44}s , *Physics Letters B* **395**, 163 (1997).

[17] A. Gade, P. Adrich, D. Bazin, B. A. Brown, J. M. Cook, C. A. Diget, T. Glasmacher, S. McDaniel, A. Ratkiewicz, K. Siwek, and D. Weisshaar, In-beam γ -ray spectroscopy of very neutron-rich nuclei: Excited states in ^{46}S and ^{48}Ar , *Phys. Rev. Lett.* **102**, 182502 (2009).

[18] L. Gaudemar, J. M. Daugas, M. Hass, S. Grévy, C. Stodel, J. C. Thomas, L. Perrot, M. Girod, B. Rossé, J. C. Angélique, D. L. Balabanski, E. Fiori, C. Force, G. Georgiev, D. Kameda, V. Kumar, R. L. Lozeva, I. Matea, V. Méot, P. Morel, B. S. N. Singh, F. Nowacki, and G. Simpson, Shell erosion and shape coexistence in $^{43}\text{S}_{27}$, *Phys. Rev. Lett.* **102**, 092501 (2009).

[19] C. Force, S. Grévy, L. Gaudemar, O. Sorlin, L. Cáceres, F. Rotaru, J. Mrazek, N. L. Achouri, J. C. Angélique, F. Azaiez, B. Bastin, R. Borcea, A. Buta, J. M. Daugas, Z. Dlouhy, Z. Dombrádi, F. De Oliveira, F. Negoita, Y. Penionzhkevich, M. G. Saint-Laurent, D. Sohler, M. Stanoiu, I. Stefan, C. Stodel, and F. Nowacki, Prolate-spherical shape coexistence at $n = 28$ in ^{44}S , *Phys. Rev. Lett.* **105**, 102501 (2010).

[20] D. Santiago-Gonzalez, I. Wiedenhöver, V. Abramkina, M. L. Avila, T. Baugher, D. Bazin, B. A. Brown, P. D. Cottle, A. Gade, T. Glasmacher, K. W. Kemper, S. McDaniel, A. Rojas, A. Ratkiewicz, R. Meharchand, E. C. Simpson, J. A. Tostevin, A. Volya, and D. Weisshaar, Triple configuration coexistence in ^{44}S , *Phys. Rev. C* **83**, 061305 (2011).

[21] B. Longfellow, D. Weisshaar, A. Gade, B. A. Brown, D. Bazin, K. W. Brown, B. Elman, J. Pereira, D. Rhodes, and M. Spieker, Quadrupole collectivity in the neutron-rich sulfur isotopes $^{38,40,42,44}\text{S}$, *Phys. Rev. C* **103**, 054309 (2021).

[22] J. J. Parker, I. Wiedenhöver, P. D. Cottle, J. Baker, D. McPherson, M. A. Riley, D. Santiago-Gonzalez, A. Volya, V. M. Bader, T. Baugher, D. Bazin, A. Gade, T. Ginter, H. Iwasaki, C. Loelius, C. Morse, F. Recchia, D. Smalley, S. R. Stroberg, K. Whitmore, D. Weisshaar, A. Lemasson, H. L. Crawford, A. O. Macchiavelli, and K. Wimmer, Isomeric character of the lowest observed 4^+ state in ^{44}S , *Phys. Rev. Lett.* **118**, 052501 (2017).

[23] F. Nowacki, A. Poves, E. Caurier, and B. Bounthong, Shape coexistence in ^{78}Ni as the portal to the fifth island of inversion, *Phys. Rev. Lett.* **117**, 272501 (2016).

[24] A. Gade, B. A. Brown, D. Bazin, C. M. Campbell, J. A. Church, D. C. Dinca, J. Enders, T. Glasmacher, M. Horoi, Z. Hu, K. W. Kemper, W. F. Mueller, T. Otsuma, L. A. Riley, B. T. Roeder, T. Suzuki, J. R. Terry, K. L. Yurkewicz, and H. Zwahlen, Evolution of the $e(1/2_1^+)-e(3/2_1^+)$ energy spacing in odd-mass k , cl , and p isotopes for $n = 20-28$, *Phys. Rev. C* **74**, 034322 (2006).

[25] L. A. Riley, D. Bazin, J. Belarge, P. C. Bender, B. A. Brown, P. D. Cottle, B. Elman, A. Gade, S. D. Gregory, E. B. Haldeman, K. W. Kemper, B. R. Klybor, M. A. Liggett, S. Lipschutz, B. Longfellow, E. Lunderberg, T. Mijatovic, J. Pereira, L. M. Skiles, R. Titus, A. Volya, D. Weisshaar, J. C. Zamora, and R. G. T. Zegers, Inverse-kinematics proton scattering from $^{42,44}\text{S}$, $^{41,43}\text{P}$, and the collapse of the $n = 28$ major shell closure, *Phys. Rev. C* **100**, 044312 (2019).

[26] V. Tripathi, B. Longfellow, A. Volya, E. Rubino, C. Benetti, J. F. Perello, S. L. Tabor, S. N. Liddick, P. C. Bender, M. P. Carpenter, J. J. Carroll, A. Chester, C. J. Chiara, K. Childers, B. R. Clark, B. P. Crider, J. T. Harke, R. Jain, S. Luitel, M. J. Mogannam, T. H. Ogunbiku, A. L. Richard, S. Saha, O. A. Shehu, R. Unz, Y. Xiao, and Y. Zhu, *Exploring β decay and β -delayed neutron emission in exotic $^{46,47}\text{Cl}$ isotopes* (2025), arXiv:2502.19378 [nucl-ex].

[27] R. Ringle, C. Bachelet, M. Block, G. Bollen, M. Facina, C. M. Folden, C. Guénaut, A. A. Kwiatkowski, D. J. Morrissey, G. K. Pang, A. M. Prinke, J. Savory, P. Schury, S. Schwarz, and C. S. Sumithrarachchi, High-precision penning trap mass measurements of neutron-rich sulfur isotopes at the $n = 28$ shell closure, *Phys. Rev. C* **80**, 064321 (2009).

[28] R. Ringle, S. Schwarz, and G. Bollen, Penning trap mass spectrometry of rare isotopes produced via projectile fragmentation at the lebit facility, *International Journal of Mass Spectrometry* **349-350**, 87 (2013), 100 years of Mass Spectrometry.

[29] M. Mukherjee, D. Beck, K. Blaum, G. Bollen, J. Dilling, S. George, F. Herfurth, A. Herlert, A. Kellerbauer, H.-J. Kluge, S. Schwarz, L. Schweikhard, and C. Yazidjian, Isoltrap: An on-line penning trap for mass spectrometry on short-lived nuclides, *The European Physical Journal A* **35**, 1 (2008).

[30] R. Wolf, F. Wienholtz, D. Atanasov, D. Beck, K. Blaum, C. Borgmann, F. Herfurth, M. Kowalska, S. Kreim, Y. A. Litvinov, D. Lunney, V. Manea, D. Neidherr, M. Rosenbusch, L. Schweikhard, J. Stanja, and K. Zuber, Isoltrap's multi-reflection time-of-flight mass separator/spectrometer, *International Journal of Mass Spectrometry* **349-350**, 123 (2013), 100 years of Mass Spectrometry.

[31] S. Bhattacharyya, M. Rejmund, A. Navin, E. Caurier, F. Nowacki, A. Poves, R. Chapman, D. O'Donnell, M. Gelin, A. Hodsdon, X. Liang, W. Mittig, G. Mukherjee, F. Rejmund, M. Rousseau, P. Roussel-Chomaz, K.-M. Spohr, and C. Theisen, Structure of neutron-rich ar isotopes beyond $n = 28$, *Phys. Rev. Lett.* **101**, 032501 (2008).

[32] A. Gade, D. Bazin, C. A. Bertulani, B. A. Brown, C. M. Campbell, J. A. Church, D. C. Dinca, J. Enders, T. Glasmacher, P. G. Hansen, Z. Hu, K. W. Kemper, W. F. Mueller, H. Olliver, B. C. Perry, L. A. Riley, B. T. Roeder, B. M. Sherrill, J. R. Terry, J. A. Tostevin, and K. L. Yurkewicz, Knockout from ^{46}Ar : $\ell = 3$ neutron removal and deviations from eikonal theory, *Phys. Rev. C* **71**, 051301 (2005).

[33] F. Sarazin, H. Savajols, W. Mittig, F. Nowacki, N. A. Orr, Z. Ren, P. Roussel-Chomaz, G. Auger, D. Bai-borodin, A. V. Belozyorov, C. Borcea, E. Caurier, Z. Dlouhý, A. Gillibert, A. S. Lalleman, M. Lewitowicz, S. M. Lukyanov, F. de Oliveira, Y. E. Penionzhkevich, D. Ridikas, H. Sakuraï, O. Tarasov, and A. de Vismes, Shape coexistence and the $N = 28$ shell closure far from stability, *Phys. Rev. Lett.* **84**, 5062 (2000).

[34] B. Jurado, H. Savajols, W. Mittig, N. Orr, P. Roussel-Chomaz, D. Baiborodin, W. Catford, M. Chartier, C. Demchonch, Z. Dlouhý, A. Gillibert, L. Giot, A. Khouaja, A. Lépine-Szily, S. Lukyanov, J. Mrazek, Y. Penionzhkevich, S. Pita, M. Rousseau, and A. Villari, Mass measurements of neutron-rich nuclei near the $n=20$ and 28 shell closures, *Physics Letters B* **649**, 43 (2007).

[35] Z. Meisel, S. George, S. Ahn, J. Browne, D. Bazin, B. A. Brown, J. F. Carpino, H. Chung, R. H. Cyburt, A. Estradé, M. Famiano, A. Gade, C. Langer, M. Matoš, W. Mittig, F. Montes, D. J. Morrissey, J. Pereira, H. Schatz, J. Schatz, M. Scott, D. Shapira, K. Smith, J. Stevens, W. Tan, O. Tarasov, S. Towers, K. Wimmer, J. R. Winkelbauer, J. Yurkon, and R. G. T. Zegers, Mass measurements demonstrate a strong $n = 28$ shell gap in argon, *Phys. Rev. Lett.* **114**, 022501 (2015).

[36] G. Bollen, R. B. Moore, G. Savard, and H. Stolzenberg, The accuracy of heavy-ion mass measurements using time of flight-ion cyclotron resonance in a penning trap, *Journal of Applied Physics* **68**, 4355 (1990), <https://doi.org/10.1063/1.346185>.

[37] S. Becker, G. Bollen, F. Kern, H.-J. Kluge, R. Moore, G. Savard, L. Schweikhard, and H. Stolzenberg, Mass measurements of very high accuracy by time-of-flight ion cyclotron resonance of ions injected into a penning trap, *International Journal of Mass Spectrometry and Ion Processes* **99**, 53 (1990).

[38] M. König, G. Bollen, H.-J. Kluge, T. Otto, and J. Szerypo, Quadrupole excitation of stored ion motion at the true cyclotron frequency, *International Journal of Mass Spectrometry and Ion Processes* **142**, 95 (1995).

[39] D. Morrissey, B. Sherrill, M. Steiner, A. Stolz, and I. Wiedenhoever, Commissioning the a1900 projectile fragment separator, *Nuclear Instruments and Methods in Physics Research Section B: Beam Interactions with Materials and Atoms* **204**, 90 (2003), 14th International Conference on Electromagnetic Isotope Separators and Techniques Related to their Applications.

[40] C. Sumithrarachchi, D. Morrissey, S. Schwarz, K. Lund, G. Bollen, R. Ringle, G. Savard, and A. Villari, Beam thermalization in a large gas catcher, *Nuclear Instruments and Methods in Physics Research Section B: Beam Interactions with Materials and Atoms* **463**, 305 (2020).

[41] K. Lund, G. Bollen, D. Lawton, D. Morrissey, J. Ottarson, R. Ringle, S. Schwarz, C. Sumithrarachchi, A. Villari, and J. Yurkon, Online tests of the advanced cryogenic gas stopper at nscl, *Nuclear Instruments and Methods in Physics Research Section B: Beam Interactions with Materials and Atoms* **463**, 378 (2020).

[42] G. Bollen, “ion surfing” with radiofrequency carpets, *International Journal of Mass Spectrometry* **299**, 131 (2011).

[43] R. Ringle, G. Bollen, A. Prinke, J. Savory, P. Schury, S. Schwarz, and T. Sun, The LEBIT 9.4T Penning trap mass spectrometer, *Nuclear Instruments and Methods in Physics Research Section A: Accelerators, Spectrometers, Detectors and Associated Equipment* **604**, 536 (2009).

[44] G. Gabrielse, Why is sideband mass spectrometry possible with ions in a penning trap?, *Phys. Rev. Lett.* **102**, 172501 (2009).

[45] R. Ringle, G. Bollen, A. Prinke, J. Savory, P. Schury, S. Schwarz, and T. Sun, A “lorentz” steerer for ion injection into a penning trap, *International Journal of Mass Spectrometry* **263**, 38 (2007).

[46] M. Kretzschmar, The ramsey method in high-precision mass spectrometry with penning traps: Theoretical foundations, *International Journal of Mass Spectrometry* **264**, 122 (2007).

[47] M. Wang, W. Huang, F. Kondev, G. Audi, and S. Naimi, The ame 2020 atomic mass evaluation (ii). tables, graphs and references*, *Chinese Physics C* **45**, 030003 (2021).

[48] F. G. Kondev, M. Wang, W. J. Huang, S. Naimi, and G. Audi, The NUBASE2020 evaluation of nuclear physics properties, *Chin. Phys. C* **45**, 030001 (2021).

[49] K. Gulyuz, J. Ariche, G. Bollen, S. Bustabad, M. Eibach, C. Izzo, S. J. Novario, M. Redshaw, R. Ringle, R. Sandler, S. Schwarz, and A. A. Valverde, Determination of the direct double- β -decay q value of ^{96}Zr and atomic masses of $^{90-92,94,96}\text{Zr}$ and $^{92,94-98,100}\text{Mo}$, *Phys. Rev. C* **91**, 055501 (2015).

[50] R. Ringle, T. Sun, G. Bollen, D. Davies, M. Facina, J. Huikari, E. Kwan, D. J. Morrissey, A. Prinke, J. Savory, P. Schury, S. Schwarz, and C. S. Sumithrarachchi, High-precision penning trap mass measurements of $^{37,38}\text{Ca}$ and their contributions to conserved vector current and isobaric mass multiplet equation, *Phys. Rev. C* **75**, 055503 (2007).

[51] K. Blaum, D. Beck, G. Bollen, P. Delahaye, C. Guénaut, F. Herfurth, A. Kellerbauer, H.-J. Kluge, D. Lunney, S. Schwarz, L. Schweikhard, and C. Yazidjian, Population inversion of nuclear states by a Penning trap mass spectrometer, *Europhysics Letters* **67**, 586 (2004).

[52] H. Hergert, A guided tour of ab initio nuclear many-body theory, *Frontiers in Physics* **8**, 10.3389/fphy.2020.00379 (2020).

[53] S. R. Stroberg, H. Hergert, J. D. Holt, S. K. Bogner, and A. Schwenk, Ground and excited states of doubly open-shell nuclei from ab initio valence-space hamiltonians, *Phys. Rev. C* **93**, 051301 (2016).

[54] S. R. Stroberg, A. Calci, H. Hergert, J. D. Holt, S. K. Bogner, R. Roth, and A. Schwenk, Nucleus-dependent valence-space approach to nuclear structure, *Phys. Rev. Lett.* **118**, 032502 (2017).

[55] S. R. Stroberg, H. Hergert, S. K. Bogner, and J. D. Holt, Nonempirical interactions for the nuclear shell model: An update, *Annual Review of Nuclear and Particle Science* **69**, 307–362 (2019).

[56] H. Hergert, S. Bogner, T. Morris, A. Schwenk, and K. Tsukiyama, The in-medium similarity renormalization group: A novel ab initio method for nuclei, *Physics Reports* **621**, 165 (2016), memorial Volume in Honor of Gerald E. Brown.